Transactions Papers

Convergence Behavior of Iteratively Decoded Parallel Concatenated Codes

Stephan ten Brink, *Member, IEEE*

***Abstract*—Mutual information transfer characteristics of soft in/soft out decoders are proposed as a tool to better understand the convergence behavior of iterative decoding schemes. The exchange of extrinsic information is visualized as a decoding trajectory in the extrinsic information transfer chart (EXIT chart). This allows the prediction of turbo cliff position and bit error rate after an arbitrary number of iterations. The influence of code memory, code polynomials as well as different constituent codes on the convergence behavior is studied for parallel concatenated codes. A code search based on the EXIT chart technique has been performed yielding new recursive systematic convolutional constituent codes exhibiting turbo cliffs at lower signal-to-noise ratios than attainable by previously known constituent codes.**

***Index Terms*—Convergence, iterative decoding, mutual information, turbo codes.**

I. Introduction

TYPICALLY, bit-error rate (BER) charts of iterative decoding schemes can be divided into three regions: 1) the region of low E_b/N_0 with negligible iterative BER reduction, 2) the turbo cliff region (also referred to as "waterfall"-region) with persistent iterative BER reduction over many iterations, and 3) the BER floor region for moderate to high E_b/N_0 in which a rather low BER can be reached after just a few number of iterations. While good analytical bounding techniques have been found for moderate to high E_b/N_0, e.g., [1]–[3], the turbo cliff has not yet attracted a comparable amount of interest, owing to the limitations of the commonly used bounding techniques in that region.

Recently, people have started to investigate the convergence behavior of iterative decoding. In [4] the authors propose a density evolution algorithm to calculate convergence thresholds for low-density parity-check (LDPC) codes on the additive white Gaussian noise (AWGN) channel; in [5], [6] density evolution is applied to construct LDPC codes with very low thresholds. The authors of [7], [8] study the convergence of iterative decoders based on signal to noise ratio (SNR) measures. A combination of SNR measures and mutual information for the description of inner rate one codes is used in [9].

This paper proposes extrinsic information transfer characteristics based on mutual information to describe the flow of extrinsic information through the soft in/soft out constituent decoders. This proves to be particularly useful in the region of low E_b/N_0. A decoding trajectory visualizes the exchange of extrinsic information between the constituent decoders in the extrinsic information transfer chart (EXIT chart).

In [10], [11] the EXIT chart was introduced as a novel tool to provide design guidelines for mappings and signal constellations of an iterative demapping and decoding scheme (IDEM). IDEM can be regarded as a serial concatenation of two codes (SCC). In this paper, the method of [10], [11] is applied to iterative decoding of parallel concatenated codes (PCC), extending the ideas of [12]. We do not claim to present a rigorous proof of stability and convergence of iterative decoding; however, simulation results suggest that the EXIT chart accurately predicts the convergence behavior of the iterative decoder for large interleaving depth.

The paper is organized as follows: Section II introduces extrinsic information transfer characteristics for the constituent decoders. Section III explains the EXIT chart as a novel description of the iterative decoder, complementary to BER charts. In Section IV we study transfer characteristics and decoding trajectories based on signal to noise ratio measures and compare them to those based on mutual information. The applicability of the EXIT chart to other than Gaussian channels is shown in Section V for the case of a Rayleigh channel. Code search results based on the EXIT chart technique are presented in Section VI yielding new constituent codes which are optimized with respect to the turbo cliff position. Finally, Section VII renders some conclusions.

II. Extrinsic Transfer Characteristics

A. Iterative Decoder for Parallel Concatenated Codes

The iterative decoder for PCC is shown in Fig. 1. For each iteration, the first constituent decoder (BCJR-algorithm [13], [14]) takes intrinsic information (channel observations) Z_1 on the systematic (information) bits i and respective parity bits p_1 and outputs soft values D_1. The extrinsic information on the systematic bits $E_1 = D_1 - A_1 - Z_1$ is passed through the bit

Paper approved by R. Koetter, the Editor for Coding Theory and Techniques of the IEEE Communications Society. Manuscript received March 30, 2000; revised December 21, 2000 and February 12, 2001. This work was carried out in a joint project with the Institute of Telecommunications (Nachrichtenübertragung), University of Stuttgart, Germany. The paper was presented in part at the 3rd IEEE/ITG Symposium on Source and Channel Coding, Munich, Germany, January 2000.

The author is with the Wireless Research Lab of Bell Laboratories, Lucent Technologies, Holmdel, NJ 07733 USA (e-mail: stenbrink@bell-labs.com).

Publisher Item Identifier S 0090-6778(01)09104-8.

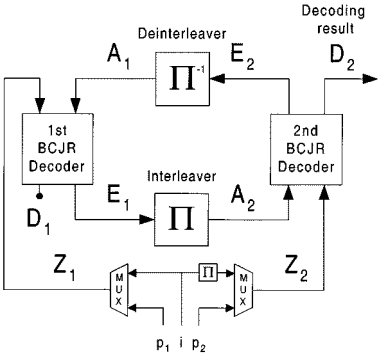

Fig. 1. Iterative decoder for parallel concatenated codes.

interleaver to become the *a priori* input A_2 of the second decoder. The second decoder takes the permuted channel observations Z_2 on the systematic bits i and respective parity bits p_2 and feeds back extrinsic information $E_2 = D_2 - A_2 - Z_2$ which becomes the *a priori* knowledge A_1 of the first decoder. The variables Z_1, A_1, D_1, E_1, Z_2, A_2, D_2 and E_2 denote log-likelihood ratios (L-values [15]).

For the received discrete-time signal from the AWGN-channel

$$z = x + n \tag{1}$$

the conditional probability density function (PDF) writes as

$$p(z|X = x) = \frac{e^{-((z-x)^2/2\sigma_n^2)}}{\sqrt{2\pi}\,\sigma_n}. \tag{2}$$

The binary random variable X denotes the transmitted bits with realizations $x \in \{\pm 1\}$; for brevity of notation, we will not distinguish between X and x in the following (only where needed for clarification). The corresponding L-values Z are calculated as

$$Z = \ln \frac{p(z|x = +1)}{p(z|x = -1)} \tag{3}$$

which can be simplified to

$$Z = \frac{2}{\sigma_n^2} \cdot z = \frac{2}{\sigma_n^2} \cdot (x + n). \tag{4}$$

The variable n is Gaussian distributed with mean zero and variance $\sigma_n^2 = N_0/2$ (double-sided noise power spectral density). Equation (4) can also be formulated as

$$Z = \mu_Z \cdot x + n_Z \tag{5}$$

with

$$\mu_Z = 2/\sigma_n^2 \tag{6}$$

and n_Z being Gaussian distributed with mean zero and variance

$$\sigma_Z^2 = 4/\sigma_n^2. \tag{7}$$

Thus, mean and variance of Z are connected by

$$\mu_Z = \frac{\sigma_Z^2}{2}. \tag{8}$$

This relationship will turn out to be useful for modeling *a priori* knowledge in the next section.

The parallel decoder of Fig. 1 is a symmetric arrangement: The situation for the second decoder with respect to Z_2, A_2, E_2 is essentially the same as for Z_1, A_1, E_1. Long sequence lengths make sure that tail effects (open/terminated trellises of convolutional codes) can be neglected. Hence, it is sufficient to focus on the first decoder for the remainder of Section II. To simplify notation the decoder index "1" is omitted in the following.

B. Transfer Characteristics of Constituent Decoders

The idea is to predict the behavior of the iterative decoder by solely looking at the input/output relations of individual constituent decoders. Since analytical treatment of the BCJR-decoder is difficult, we make use of the following observations obtained by simulation. 1) For large interleavers the *a priori* values A remain fairly uncorrelated from the respective channel observations Z over many iterations. 2) The probability density functions of the extrinsic output values E (*a priori* values A for the next decoder respectively) approach Gaussian-like distributions with increasing number of iterations, as already observed in [16].

An explanation for the first observation can be found by looking at the decoder output $D = Z + A + E$. For soft in/soft out decoding with the BCJR-algorithm the extrinsic information E_k of the bit at time instance k is not influenced by the channel observations Z_k or *a priori* knowledge A_k [17]. A large interleaver further contributes to reduce correlations and to get a better "separation" of both decoders. Possible reasons for the second observation are a) the use of a Gaussian channel model, and b) that sums over many values are involved in the L-value calculation of E which typically leads to Gaussian-like distributions.

Observations 1 and 2 suggest that the *a priori* input A to the constituent decoder can be modeled by applying an independent Gaussian random variable n_A with variance σ_A^2 and mean zero in conjunction with the known transmitted systematic bits x.

$$A = \mu_A \cdot x + n_A. \tag{9}$$

Since A is supposed to be an L-value based on Gaussian distributions, as in the case of (5), (8), the mean value μ_A must fulfill

$$\mu_A = \frac{\sigma_A^2}{2}. \tag{10}$$

With (10) the conditional probability density function belonging to the L-value A is

$$p_A(\xi|X = x) = \frac{e^{-((\xi-(\sigma_A^2/2)\cdot x)^2)/2\sigma_A^2)}}{\sqrt{2\pi}\,\sigma_A}. \tag{11}$$

Note that (10) can also be derived using the consistency condition [4] for the L-value distribution, $p_A(\xi|X = x) = p_A(-\xi|X = x) \cdot e^{x\cdot\xi}$.

To measure the information contents of the *a priori* knowledge, mutual information $I_A = I(X; A)$ [18], [19] between transmitted systematic bits X and the L-values A is used.

$$I_A = \frac{1}{2} \cdot \sum_{x=-1,1} \int_{-\infty}^{+\infty} p_A(\xi|X = x) \times \mathrm{ld}\,\frac{2 \cdot p_A(\xi|X = x)}{p_A(\xi|X = -1) + p_A(\xi|X = 1)}\, d\xi \tag{12}$$

$$0 \le I_A \le 1. \tag{13}$$

With (11), (12) becomes

$$I_A(\sigma_A) = 1 - \int_{-\infty}^{\infty} \frac{e^{-((\xi-\sigma_A^2/2)^2/2\sigma_A^2)}}{\sqrt{2\pi}\,\sigma_A} \cdot \mathrm{ld}\,[1+e^{-\xi}]\,d\xi. \quad (14)$$

For abbreviation we define

$$J(\sigma) := I_A(\sigma_A = \sigma) \quad (15)$$

with

$$\lim_{\sigma\to 0} J(\sigma) = 0, \quad \lim_{\sigma\to\infty} J(\sigma) = 1, \qquad \sigma > 0. \quad (16)$$

With (4)–(7) we realize that the capacity of the binary input/continuous output AWGN channel of (1) is given by

$$C_G = J(\sigma = 2/\sigma_n). \quad (17)$$

The capacity C_G [the function $J(\sigma)$ respectively] cannot be expressed in closed form. It is monotonically increasing [18] in $\sigma = 2/\sigma_n$ and thus reversible.

$$\sigma_A = J^{-1}(I_A). \quad (18)$$

Mutual information is also used to quantify the extrinsic output $I_E = I(X; E)$.

$$I_E = \frac{1}{2} \cdot \sum_{x=-1,\,1} \int_{-\infty}^{+\infty} p_E(\xi|X=x) \times \mathrm{ld}\frac{2 \cdot p_E(\xi|X=x)}{p_E(\xi|X=-1) + p_E(\xi|X=1)}\,d\xi \quad (19)$$

$$0 \le I_E \le 1. \quad (20)$$

Viewing I_E as a function of I_A and the E_b/N_0-value, the extrinsic information transfer characteristics are defined as

$$I_E = T(I_A,\, E_b/N_0) \quad (21)$$

or, for fixed E_b/N_0, just

$$I_E = T(I_A). \quad (22)$$

To compute $T(I_A,\, E_b/N_0)$ for the desired $(I_A,\, E_b/N_0)$-input combination, the distributions p_E of (19) are most conveniently determined by Monte Carlo simulation (histogram measurements). For this, the independent Gaussian random variable of (9) is applied as *a priori* input to the constituent decoder of interest; a certain value of I_A is obtained by appropriately choosing the parameter σ_A according to (18). Sequence lengths of 10^4 systematic bits were found to sufficiently suppress tail effects. Note that no Gaussian assumption is imposed on the extrinsic output distributions p_E.

Transfer characteristics $I_E = T(I_A,\, E_b/N_0)$ are given in Fig. 2. The *a priori* input I_A is on the abscissa, the extrinsic output I_E on the ordinate. The E_b/N_0-value serves as a parameter to the curves. The BCJR-algorithm is applied to a rate 1/2 recursive systematic convolutional code of memory 4; the parity bits are punctured to obtain a rate 2/3 constituent code. This will lead to a rate 1/2 PCC in Section III. The code polynomials are $(G_r,\, G) = (023,\, 037)$. G_r stands for the (recursive) feedback polynomial; the values are given in octal, with the most significant bit (MSB) corresponding to the generator connection on the very left (input) side of the shift register. Note that the E_b/N_0-values are given with respect to the rate 1/2 parallel concatenated code.

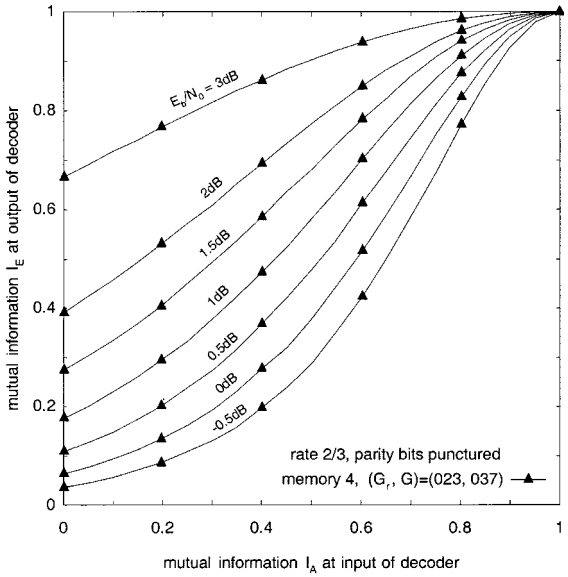

Fig. 2. Extrinsic information transfer characteristics of soft in/soft out decoder for rate 2/3 convolutional code; E_b/N_0 of channel observations serves as parameter to curves.

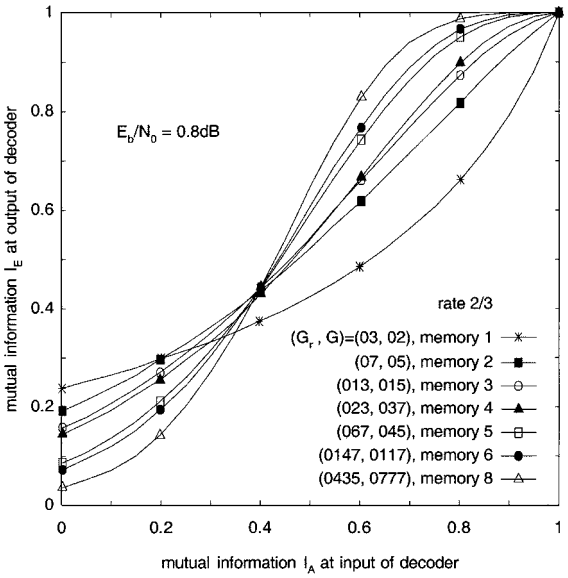

Fig. 3. Extrinsic information transfer characteristics of soft in/soft out decoder for rate 2/3 convolutional code, $E_b/N_0 = 0.8$ dB, different code memory.

Transfer characteristics for different code memory at fixed $E_b/N_0 = 0.8$ dB are depicted in Fig. 3. The code polynomials are taken from [20].

Fig. 4 shows the influence of different code polynomials for the prominent case of a memory 4 code. The (023, 011)-code provides good extrinsic output at the beginning, but returns diminishing output for higher *a priori* input. For the (023, 035)-code it is the other way round. The constituent code of the classic rate 1/2 PCC of [21] with polynomials (037, 021) has good extrinsic output for low to medium *a priori* input.

From Figs. 2–4 it can be seen that the characteristics $I_E = T(I_A)$ are monotonically increasing in I_A, $0 \le I_A \le 1$, and thus the inverse function

$$I_A = T^{-1}(I_E) \quad (23)$$

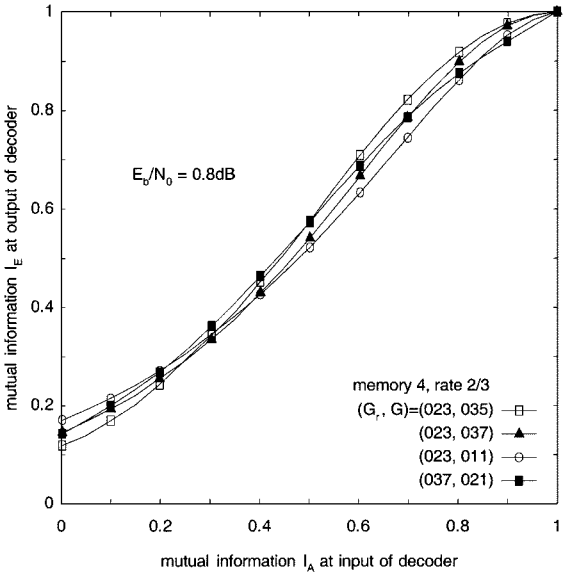

Fig. 4. Extrinsic information transfer characteristics of soft in/soft out decoder for rate 2/3 convolutional code, $E_b/N_0 = 0.8$ dB, memory 4, different code polynomials.

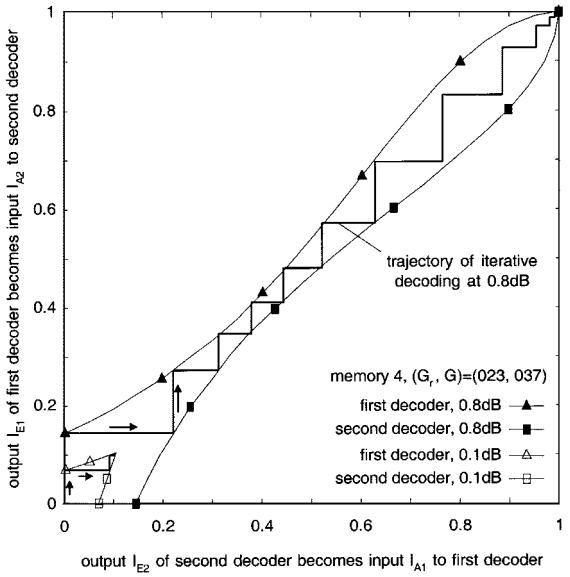

Fig. 5. Simulated trajectories of iterative decoding at $E_b/N_0 = 0.1$ dB and 0.8 dB (symmetric PCC rate 1/2, interleaver size 60 000 systematic bits).

exists on

$$T(0) \le I_E \le T(1). \tag{24}$$

Increasing I_A means that more and more bits X become known at the decoder with high confidence, which relates to a growing conditioning of the mutual information $I_E = I(X; E)$ on the *a priori* knowledge. As conditioning increases mutual information [18] it is plausible that bigger *a priori* input provides bigger extrinsic output.

III. Extrinsic Information Transfer Chart

A. Trajectories of Iterative Decoding

To account for the iterative nature of the suboptimal decoding algorithm, both decoder characteristics are plotted into a single diagram. However, for the transfer characteristics of the second decoder the axes are swapped.

This diagram is referred to as EXIT chart since the exchange of extrinsic information can be visualized as a decoding trajectory.

Let n be the iteration index, E_b/N_0 fixed. For $n = 0$ the iteration starts at the origin with zero *a priori* knowledge $I_{A_1,0} = 0$. At iteration n, the extrinsic output of the first decoder is $I_{E_1,n} = T_1(I_{A_1,n})$. $I_{E_1,n}$ is forwarded to the second decoder to become $I_{A_2,n} = I_{E_1,n}$ (ordinate). The extrinsic output of the second decoder is $I_{E_2,n} = T_2(I_{A_2,n})$, which is fed back to the first decoder to become the *a priori* knowledge $I_{A_1,n+1} = I_{E_2,n}$ (abscissa) of the next iteration. Note that interleaving does not change mutual information.

The iteration proceeds as long as $I_{E_2,n+1} > I_{E_2,n}$. With $I_{E_2,n+1} = T_2(T_1(I_{E_2,n}))$ this can be formulated as $T_1(I_{E_2,n}) > T_2^{-1}(I_{E_2,n})$. The iteration stops if $I_{E_2,n+1} = I_{E_2,n}$, or equivalently, $T_1(I_{E_2,n}) = T_2^{-1}(I_{E_2,n})$, which corresponds to an intersection of both characteristics in the EXIT chart.

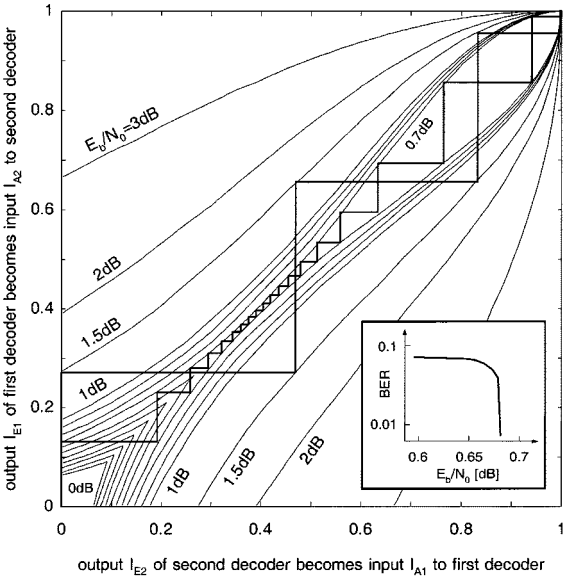

Fig. 6. EXIT chart with transfer characteristics for a set of E_b/N_0-values; two decoding trajectories at 0.7 dB and 1.5 dB (code parameters as in Fig. 5, PCC rate 1/2); interleaver size 10^6 bits.

Fig. 5 shows trajectories of iterative decoding at $E_b/N_0 = 0.1$ dB and 0.8 dB (code parameters are those of Fig. 2). The trajectory is a simulation result taken from the "free-running" iterative decoder. For $E_b/N_0 = 0.1$ dB the trajectory (lower left corner) gets stuck after two iterations since both decoder characteristics do intersect. For $E_b/N_0 = 0.8$ dB the trajectory has just managed to "sneak through the bottleneck." After six passes through the decoder, increasing correlations of extrinsic information start to show up and let the trajectory deviate from its expected zigzag-path. As it turns out, for larger interleavers the trajectory stays on the characteristics for some more passes through the decoder.

Fig. 6 depicts the EXIT chart with transfer characteristics over a set of E_b/N_0-values. The curves in between 0 dB and

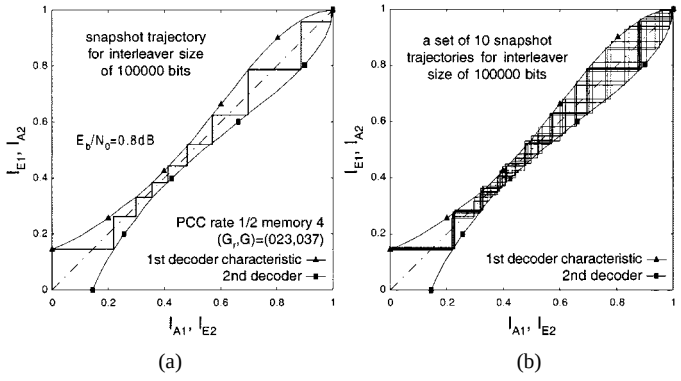

Fig. 7. Transition from snapshot trajectory to averaged trajectory; $E_b/N_0 = 0.8$ dB; PCC rate 1/2 memory 4, $(G_r, G) = (023, 037)$; interleaver size 10^5 bits.

1 dB are in steps of 0.1 dB. Note that in the graphical representation the decoder characteristics are only plotted up to their first intersection, in order not to overload the two-dimensional graph. An opening for the trajectory at 0.7 dB can clearly be seen, which corresponds to the turbo cliff position in the BER chart.

Considering the behavior of the decoding trajectory in the EXIT chart we can come up with a more vivid nomenclature for the three typical regions of the BER chart. 1) The region of low E_b/N_0 with negligible iterative BER reduction can also be referred to as the *pinch-off region* with the decoder transfer characteristics intersecting at low mutual information (corresponding to high BER) and the trajectory getting stuck. 2) The turbo cliff region is now the *bottleneck region* with the decoding trajectory just managing to sneak through a narrow tunnel; convergence toward low BER is slow, but possible since both decoder characteristics do not intersect anymore. 3) The BER floor region can also be regarded as the *wide-open region* with fast convergence. Likewise, the acronym EXIT can be understood as the opportunity to see at what E_b/N_0 the decoding trajectory succeeds in "exiting" the pinch-off region through the bottleneck to converge toward low BER.

The main contribution of the EXIT chart to the understanding of iterative decoding is the advantage that only simulations of individual constituent decoders are needed to obtain the desired transfer characteristics. These can then be used in any combination in the EXIT chart to describe the behavior of the corresponding iterative decoder, asymptotic with respect to the interleaver size. No resource-intensive BER simulations of the iterative decoding scheme itself are required.

B. Snapshot and Averaged Trajectory

As the iterative decoding is block-oriented, we can further distinguish between *snapshot trajectory* and *averaged trajectory.* For the *snapshot trajectory,* the measurements of extrinsic output PDFs $p_{E,n}$ at iteration n stem from the iterative decoding of a *single* block (Fig. 6 shows snapshot trajectories). For the *averaged trajectory,* the extrinsic output PDFs are *averaged* over a number of N_B blocks applying

$$\overline{p_{E,n}(\xi|X=\pm 1)} = \frac{1}{N_B} \cdot \sum_{b=1}^{N_B} p_{E,n,b}(\xi|X=\pm 1) \qquad (25)$$

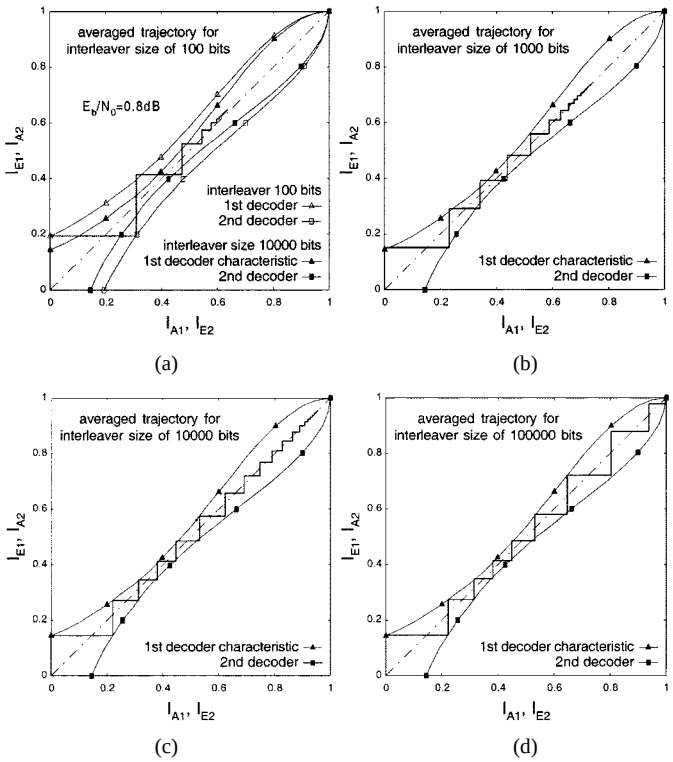

Fig. 8. Averaged decoding trajectories for different interleaver lengths; PCC rate 1/2 memory 4, $(G_r, G) = (023, 037)$; averaged over 10^8 information bits.

to trace an average behavior of the decoding convergence in the EXIT chart (Fig. 5 shows averaged trajectories).

Fig. 7 further illustrates these concepts. The left EXIT chart contains a snapshot trajectory for a rate 1/2 PCC obtained by measuring the decoding convergence of a single block of $2 \cdot 10^5$ bits. In the right EXIT chart a set of 10 decoding trajectories is shown, obtained from simulation of 10 different blocks of $2 \cdot 10^5$ bits. As the interleaving depth is quite big, the decoding trajectories do already match fairly well with the transfer characteristics; however, small deviations at the beginning can accumulate to big differences among the trajectories after some iterations.

The quantity of these variations is characterized by the averaged trajectory which is depicted in Fig. 8 for different interleaving depth: The bigger the variations of the "per block"-snapshot trajectories, the bigger the mismatch of averaged trajectory and transfer characteristics. For short interleaver size, increasing correlations of extrinsic information let the averaged trajectory literally "die out" after some iterations. As we increase the interleaver size from 10^2 (top left) to 10^5 bits (bottom right), the agreement of averaged trajectory and decoder transfer characteristics gradually improves.

For a very short interleaver size of 100 bits (top left EXIT chart) we also notice the following two effects: 1) The trellis termination shows up; the symmetry axis of the trajectory is shifted away from the EXIT chart diagonal, more toward the extrinsic output of the first constituent decoder, which is the one using trellis termination (for simplicity, the second trellis is left open). 2) For the first few iterations the extrinsic output traced by the trajectory turns out to be bigger than expected for both terminated and unterminated trellis decoding; apparently,

for short sequence length it is easier for the BCJR decoder to gain new, extrinsic information on the systematic bits.

C. Obtaining BER From EXIT Chart

The EXIT chart can be used to obtain an estimate on the BER after an arbitrary number of iterations. For both constituent decoders, the soft output on the systematic bits can be written as $D = Z + A + E$. For the sake of deriving a simple formula on the bit error probability P_b, we assume the *a priori* knowledge A and extrinsic output E to be Gaussian distributed. Consequently, the decoder soft output D is supposed to be Gaussian distributed with variance σ_D^2 and mean value $\mu_D = \sigma_D^2/2$, compare to (8), (10). With the complementary error function, the bit error probability writes as

$$P_b \approx \frac{1}{2}\operatorname{erfc}\left(\frac{1}{\sqrt{2}}\,\frac{\mu_D}{\sigma_D}\right) = \frac{1}{2}\operatorname{erfc}\left(\frac{\sigma_D}{2\sqrt{2}}\right). \tag{26}$$

Assuming independence it is

$$\sigma_D^2 = \sigma_Z^2 + \sigma_A^2 + \sigma_E^2. \tag{27}$$

With (4) and

$$\frac{E_b}{N_0} = \frac{1}{2R\sigma_n^2} \tag{28}$$

we obtain σ_Z^2 as

$$\sigma_Z^2 = \left(\frac{2}{\sigma_n^2}\cdot\sigma_n\right)^2 = \frac{4}{\sigma_n^2} = 8R\cdot\frac{E_b}{N_0}. \tag{29}$$

Applying (18), the variances σ_A^2 and σ_E^2 are calculated.

$$\sigma_A^2 \approx J^{-1}(I_A)^2, \quad \sigma_E^2 \approx J^{-1}(I_E)^2. \tag{30}$$

Finally, with (26), (27), (29), and (30) the result is

$$P_b \approx \frac{1}{2}\operatorname{erfc}\left(\frac{\sqrt{8R\cdot\dfrac{E_b}{N_0} + J^{-1}(I_A)^2 + J^{-1}(I_E)^2}}{2\sqrt{2}}\right). \tag{31}$$

Fig. 9 shows transfer characteristics and respective simulated decoding trajectory of an asymmetric PCC with memory 2 and memory 6 constituent codes at 0.8 dB. Note that the transfer characteristics are just taken from Fig. 3; the characteristic of the second decoder (memory 6) is mirrored at the first diagonal of the EXIT chart. Additionally, the BER scaling according to (31) is given as a contour plot. Table I compares BER-results obtained from the EXIT chart up to the seventh pass through the iterative decoder: (s) stands for the result obtained by simulation, right next to it the BER as calculated with (31). The table shows that the EXIT chart in combination with the Gaussian approximation of (31) provides reliable BER predictions down to 10^{-3}, that is, in the region of low E_b/N_0. It is not useful for determining BER floors. For this bounding techniques like [1] which include the interleaving depth are more suited.

IV. Mutual Information Versus SNR Measures

A. Different SNR Measures

There are several ways of defining SNR measures, depending on whether and how a Gaussian assumption is included. In the following we consider three different SNR measures.

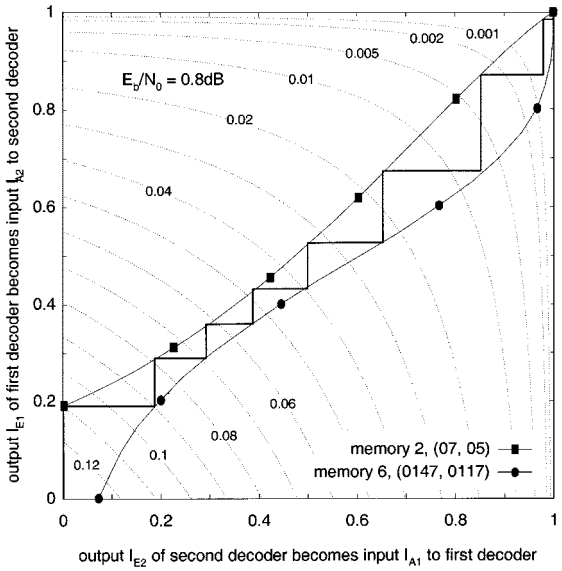

Fig. 9. Averaged trajectory at $E_b/N_0 = 0.8$ dB with BER scaling as contour plot (PCC rate $1/2$, interleaver size $2\cdot 10^5$ bits).

TABLE I
Comparison of BER Predictions From EXIT Chart. Columns of Simulation Results are Marked With (s)

	1st decoder		2nd decoder	
pass	BER (s)	BER (31)	BER (s)	BER (31)
1.	1.10e-1	1.10e-1	8.96e-2	8.97e-2
2.	7.86e-2	7.88e-2	6.85e-2	6.88e-2
3.	6.18e-2	6.21e-2	5.37e-2	5.39e-2
4.	4.78e-2	4.80e-2	3.94e-2	3.95e-2
5.	3.30e-2	3.31e-2	2.32e-2	2.32e-2
6.	1.65e-2	1.62e-2	7.63e-3	7.08e-3
7.	3.65e-3	2.95e-3	7.0e-4	4.4e-4

1) The unbiased SNR $\gamma_{E,(\mu,\sigma)}$ is based on the mean and the variance of the measured extrinsic output PDF p_E; no Gaussian assumption on p_E is made.

$$\gamma_{E,(\mu,\sigma)} = \frac{\mu_E^2}{\sigma_E^2}. \tag{32}$$

For linear codes on the AWGN channel, the communication link with encoder, channel and decoder is symmetric in $X = \pm 1$; pragmatically, we make use of both histogram measurements $p_E(\xi|X=-1)$, $p_E(\xi|X=1)$ to obtain a better averageing of the Monte Carlo simulation results. The mean value is measured by

$$\mu_E = \tfrac{1}{2}\int_{-\infty}^{\infty}\xi\cdot[p_E(\xi|X=1) - p_E(\xi|X=-1)]\,d\xi \tag{33}$$

and the variance

$$\sigma_E^2 = \tfrac{1}{2}\int_{-\infty}^{\infty}\xi^2\cdot[p_E(\xi|X=1) + p_E(\xi|X=-1)]\,d\xi - \mu_E^2. \tag{34}$$

2) The biased SNR $\gamma_{E,(\mu)}$ is based only on the mean value μ_E of the PDF p_E; the mean μ_E is assumed to be the

mean value of a Gaussian distributed L-value, with $\mu_E = \mu_{E,G} = \sigma^2_{E,G}/2$, according to (10).

$$\gamma_{E,(\mu)} = \frac{\mu_E^2}{\sigma^2_{E,G}} = \frac{\mu_E^2}{2\mu_E} = \frac{\mu_E}{2}. \tag{35}$$

Hence, the Gaussian assumption on the PDF p_E eliminates the necessity of measuring the actual variance σ^2_E with (34), which is different from the imposed variance $\sigma^2_{E,G}$.

3) The biased SNR $\gamma_{E,(P_b)}$ is based on the error probability of the extrinsic output. The Gaussian assumption comes into play by inverting the Q-function (or erfc-function) for finding the corresponding SNR value.

$$\gamma_{E,(P_b)} = [Q^{-1}(P_b)]^2 = 2[\mathrm{erfc}^{-1}(2P_b)]^2. \tag{36}$$

The error probability with respect to the extrinsic output is

$$P_b = \tfrac{1}{2}\int_{-\infty}^{0} p_E(\xi|X=1)d\xi + \tfrac{1}{2}\int_{0}^{\infty} p_E(\xi|X=-1)\,d\xi. \tag{37}$$

It is not necessary to perform a histogram measurement of p_E; just counting the bit errors of the extrinsic L-values is sufficient which is numerically more convenient.

B. Predicted versus Actual Iterative Decoding Behavior

The choice of the particular code example is arbitrary; we chose the classic rate 1/2 memory 4 code [21] with polynomials $(G_r, G) = (037, 021)$, yielding typical results comparable to other PCC examples.

Fig. 10 compares the EXIT chart predictions based on transfer characteristics with the actual iterative decoding behavior described by the trajectory. An agreement of transfer characteristics and decoding trajectory indicates that the respective measure allows an accurate prediction of the E_b/N_0-decoding threshold. It is important to mention that the characteristics and trajectories of Fig. 10 are based on the *same* simulation results for p_E, and just *different ways* of interpreting and visualizing the measured data according to (32), (35), (36), and (19) are chosen.

The unbiased SNR measure $\gamma_{E,(\mu,\sigma)}$ is used in the upper left EXIT chart of Fig. 10. The intersection of both transfer characteristics at $E_b/N_0 = 0.6$ dB suggests that no convergence is possible. However, the actual behavior of the iterative decoder, represented by the decoding trajectory, shows convergence toward low BER; transfer characteristics and decoding trajectory do not match. Consequently, E_b/N_0-convergence threshold values based on $\gamma_{E,(\mu,\sigma)}$ tend to be too pessimistic; a similar behavior can be observed for the EXIT chart in the lower left corner, applying the biased SNR $\gamma_{E,(P_b)}$. Threshold values based on $\gamma_{E,(\mu)}$ (upper right EXIT chart) are too optimistic: The transfer characteristics indicate a wider convergence tunnel than actually seen by the decoding trajectory.

The lower right corner depicts the EXIT chart using the mutual information measure. Transfer characteristics and decoding trajectory are in good agreement, indicating that convergence thresholds (pinch-off limits $E_b/N_0|_{\mathrm{off}}$) based on mutual information are very close to the actual threshold values as obtainable from density evolution [4]. Table II summarizes the threshold predictions for this particular code example. The threshold value

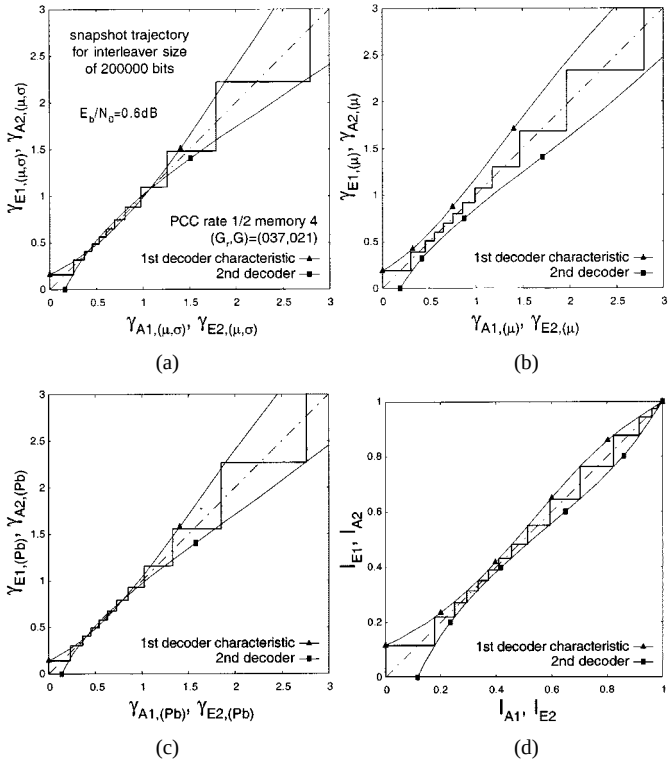

Fig. 10. Transfer characteristics and snapshot trajectories for different SNR measures in comparison to mutual information; $E_b/N_0 = 0.6$ dB; PCC rate 1/2 memory 4, $(G_r, G) = (037, 021)$; interleaver size $2 \cdot 10^5$ bits.

TABLE II
COMPARISON OF CONVERGENCE THRESHOLD PREDICTIONS FOR PCC OF RATE 1/2 MEMORY 4, $(G_r, G) = (037, 021)$

	predicted threshold [dB]
$E_b/N_0\|_{\mathrm{off},\gamma_{E,(\mu)}}$	0.41
$E_b/N_0\|_{\mathrm{off,DE}}$	0.537
$E_b/N_0\|_{\mathrm{off}}$	0.53
$E_b/N_0\|_{\mathrm{off},\gamma_{E,(P_b)}}$	0.65
$E_b/N_0\|_{\mathrm{off},\gamma_{E,(\mu,\sigma)}}$	0.69

$E_b/N_0|_{\mathrm{off,\,DE}}$ was gained from density evolution and is taken from [22].

In addition to the good threshold prediction capabilities we find the following properties of mutual information advantageous in comparison to SNR measures: 1) *The numerical stability*: For the BCJR algorithm, the forward and backward probabilities ("alpha"-, "beta"-values, e.g., [14]) can be regarded as accumulated path metrics. To avoid mantissa saturation of the floating point arithmetic for long sequence lengths, the extrinsic L-values need to be clipped to, say, ± 50 prior to becoming *a priori* knowledge for the successive decoding step. This causes a distortion of the SNR measures $\gamma_{E,(\mu,\sigma)}$ and $\gamma_{E,(\mu)}$, resulting in smaller SNR values. As the *overlap* of both PDF's $p_E(\xi|X=-1), p_E(\xi|X=1)$ at low reliability values dominates the mutual information measure, it remains practically unaffected by clipping. 2) *The information-theoretic interpretation*: According to Shannon's

channel coding theorem, mutual information between channel input and output variable directly relates to the maximal possible information rate for which reliable (i.e., error-free) transmission is achievable. This interpretation turns out to be particularly useful for serially concatenated coding schemes like presented in [10], [23] where mutual information characterizes the properties of different constellation mappings. 3) *The value range and logarithmic scaling*: Mutual information per binary symbol stays within the interval $[0 \cdots 1]$ while covering the entire range from zero to perfect knowledge on the transmitted bits. This makes it convenient to plot in a square chart with equally scaled abscissa and ordinate.

V. Exit Chart for the Rayleigh Channel

The EXIT chart technique is not limited to the Gaussian channel. In this section we explain the changes for a coherently detected, fully interleaved Rayleigh channel when perfect channel state information is available at the receiver. The received discrete-time signal is

$$z_c = a_c \cdot x + n_c \tag{38}$$

with the transmitted binary symbols $x \in \{\pm 1\}$ and the complex additive noise $n_c = n_I + jn_Q$. The n_I, n_Q are realizations of independent Gaussian random variables with variance $\sigma_n^2 = N_0/2$. The complex fading coefficient is $a_c = a_I + ja_Q$. The a_I, a_Q are Gaussian distributed; their variance is normalized to $\sigma_a^2 = 1/2$ such that the magnitude $a = \sqrt{a_I^2 + a_Q^2}$ is Rayleigh distributed with $E[a^2] = 1$.

Assuming perfectly known a_c at the receiver the channel L-values are calculated as

$$Z = \ln \frac{p(z_c|a_c,\, x=+1)}{p(z_c|a_c,\, x=-1)} \tag{39}$$

with

$$p(z_c|a_c,\, x) = \frac{1}{2\pi\sigma_n^2} \exp\left[-\frac{|z_c - a_c \cdot x|^2}{2\sigma_n^2}\right] \tag{40}$$

which results in

$$Z = \frac{2}{\sigma_n^2} \cdot \mathrm{Re}\{a_c^* \cdot z_c\} = \frac{2}{\sigma_n^2} \cdot (a^2 \cdot x + a \cdot n). \tag{41}$$

It is straightforward to show that n is Gaussian distributed with variance σ_n^2 and mean zero.

A. Extrinsic Transfer Characteristics

We noticed that the shapes of the extrinsic density functions at the decoder output are similar to those of the Gaussian channel case. Hence, following the same arguments as in Section II-B, we model the *a priori* knowledge A as an independent Gaussian random variable according to (9). Likewise, the extrinsic information transfer characteristics $I_E = T_R(I_A, E_b/N_0)$ for the Rayleigh channel are computed by Monte Carlo simulation applying (12) and (19) in combination with the (no longer Gaussian distributed) channel L-values Z of (41). As for the Gaussian channel case, we found a very good agreement of transfer characteristics and simulated decoding trajectories.

B. Obtaining BER From EXIT Chart

The probability density function of the channel L-values Z can be calculated from (40) and (41) using integral [24, (3.325)].

$$p_Z(t|x) = \frac{\sigma_n^2}{2\sqrt{1+2\sigma_n^2}} \cdot \exp\left[\frac{x \cdot t}{2} - \sqrt{1+2\sigma_n^2} \cdot \frac{|t|}{2}\right]. \tag{42}$$

As in Section III-C, the decoder soft output D can be written as a sum of independent random variables $D = Z + A + E$, with the *a priori* values A and extrinsic output values E being approximated by independent Gaussian random variables. Thus, the sum $A + E$ itself is Gaussian distributed with variance $\sigma_{AE}^2 = \sigma_A^2 + \sigma_E^2$, mean value $\mu_{AE} = \sigma_{AE}^2/2$ and probability density function

$$p_{AE}(t|x) = \frac{1}{\sqrt{2\pi}\,\sigma_{AE}} \cdot \exp\left[\frac{1}{2\sigma_{AE}^2} \cdot \left(t - \frac{\sigma_{AE}^2}{2} \cdot x\right)^2\right]. \tag{43}$$

The PDF p_D of the sum $Z + A + E$ is calculated through convolution of (42) and (43)

$$p_D(t|x) = p_Z(t|x) * p_{AE}(t|x). \tag{44}$$

With integral [24, (3.322, 2.)] we obtain

$$\begin{aligned} p_D(t|x) = {} & \frac{\sigma_n^2}{4\sqrt{1+2\sigma_n^2}} \cdot \exp\left(\frac{\sigma_n^2\sigma_{AE}^2}{4}\right) \\ & \times \left[\exp\left(\frac{1+\sqrt{1+2\sigma_n^2}}{2} \cdot x \cdot t\right)\right. \\ & \times \mathrm{erfc}\left(\frac{1}{\sqrt{2}\,\sigma_{AE}} \cdot x \cdot t + \frac{\sigma_{AE} \cdot \sqrt{1+2\sigma_n^2}}{2\sqrt{2}}\right) \\ & + \exp\left(\frac{1-\sqrt{1+2\sigma_n^2}}{2} \cdot x \cdot t\right) \\ & \left. \times\, \mathrm{erfc}\left(-\frac{1}{\sqrt{2}\,\sigma_{AE}} \cdot x \cdot t + \frac{\sigma_{AE} \cdot \sqrt{1+2\sigma_n^2}}{2\sqrt{2}}\right)\right]. \end{aligned} \tag{45}$$

The bit error probability is calculated from (45) by integration

$$P_b = \int_{-\infty}^{0} p_D(t|x=1)\, dt. \tag{46}$$

Applying integral [24, (6.282, 1.)] gives rise to the following closed-form result

$$\begin{aligned} P_b = {} & \frac{1}{2}\,\mathrm{erfc}\left(\frac{\sigma_{AE}}{2\sqrt{2}}\right) - \frac{1}{2}\,\mathrm{erfc}\left(\frac{\sigma_{AE}\sqrt{1+2\sigma_n^2}}{2\sqrt{2}}\right) \\ & \times \frac{1}{\sqrt{1+2\sigma_n^2}} \cdot \exp\left[\frac{\sigma_n^2\sigma_{AE}^2}{4}\right]. \end{aligned} \tag{47}$$

With (28), (47) and $\sigma_{AE}^2 \approx J^{-1}(I_A)^2 + J^{-1}(I_E)^2$ an estimate on the BER can be obtained from the EXIT chart. For the simulated decoding trajectory of Fig. 11 the same constituent code combination as in Fig. 9 is used. Additionally, we chose $E_b/N_0 = 2.6$ dB such that the distance to the capacity limit is comparable to the Gaussian channel case of Fig. 9: For rate 1/2, the capacity limit of the Rayleigh channel is at 1.83 dB, and thus the distance is 2.6 dB $-$ 1.73 dB $=$ 0.77 dB; for the Gaussian channel the capacity limit is at 0.19 dB and the distance is 0.8 dB $-$ 0.19 dB $=$ 0.61 dB. The BER obtained from (47) is given

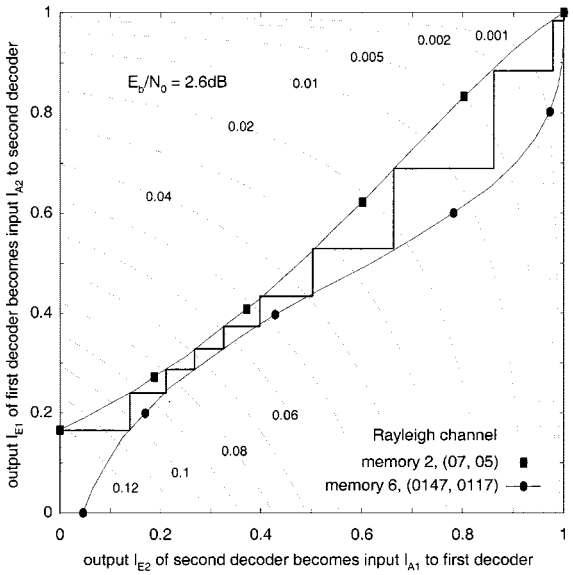

Fig. 11. Averaged trajectory of iterative decoding at $E_b/N_0 = 2.6$ dB with BER scaling as contour plot (PCC rate 1/2, interleaver size $2 \cdot 10^5$ bits); Rayleigh channel.

TABLE III
COMPARISON OF BER PREDICTIONS (RAYLEIGH CHANNEL). COLUMNS OF SIMULATION RESULTS ARE MARKED WITH (s).

	1st decoder		2nd decoder	
pass	BER (s)	BER (47)	BER (s)	BER (47)
1.	1.23e-1	1.22e-1	1.05e-1	1.03e-1
2.	9.44e-2	9.30e-2	8.60e-2	8.48e-2
3.	8.00e-2	7.92e-2	7.42e-2	7.33e-2
4.	6.95e-2	6.89e-2	6.41e-2	6.33e-2
5.	5.90e-2	5.89e-2	5.31e-2	5.25e-2
6.	4.81e-2	4.74e-2	3.95e-2	3.91e-2
7.	3.32e-2	3.26e-2	2.34e-2	2.22e-2
8.	1.63e-2	1.48e-2	7.24e-3	6.21e-3
9.	3.86e-3	2.42e-3	9.5e-4	4.05e-4

as contour lines. As indicated in Table III, the BER predictions are quite accurate down to 10^{-3}.

VI. APPLICATIONS OF THE EXIT CHART

A. Tables of Pinch-Off Limits

The results of Figs. 2–4 can be reinterpreted in the EXIT chart. Obviously, with respect to Fig. 3, a big code memory hurts at the beginning of the iteration, but helps for reaching a low BER floor. Table IV gives an overview of the pinch-off limits for symmetric (entries on diagonal of table) and asymmetric PCC of rate 1/2 using the constituent codes of Fig. 3.

B. Search for "Early Converging" Codes

There have been various code searches for parallel concatenated codes focusing on optimizing "effective" free distances of constituent codes and multiplicities thereof [20], [25]. While these quantities govern the code performance in the BER floor region, they have only little influence on the convergence properties in the turbo cliff region. Table V shows the result of a code search over PCC of code rate 1/2 (rate 1/2 constituent codes punctured to rate 2/3) and rate 1/3 up to memory 6. We restricted ourselves to symmetric PCC. The extrinsic transfer characteristic of the respective constituent decoder must not intersect with the first diagonal of the EXIT chart, or equivalently, $I_E > I_A$ must be fulfilled for $0 < I_A < 1$. We demanded convergence to low BER at 0.5 dB for the rate 1/2 PCC (0.31 dB away from Gaussian capacity limit 0.19 dB), and at -0.2 dB for the rate 1/3 PCC (0.3 dB away from capacity limit -0.5 dB). We relaxed the convergence-criterion and allowed intersections of transfer characteristics above $I_A > 0.9$ such that bit error rates of about 10^{-3} and better can be reached. No code with memory smaller than 4 could meet these requirements.

Two memory 6 codes of Table V exhibit a remarkable property: After overcoming a first bottleneck-like threshold (intersection at low to medium mutual information, BER $\approx 5 \cdot 10^{-2}$), a second threshold shows up (intersection at high mutual information, BER $\approx 10^{-3}$), preventing the iterative decoder from

TABLE IV
PINCH-OFF LIMITS $E_b/N_0|_{\text{off}}$ [dB] FOR PCC OF RATE 1/2 USING THE CONSTITUENT CODES OF FIG. 3; GAUSSIAN CHANNEL

first decoder	second decoder					
(G_r, G)	C_1	C_2	C_3	C_4	C_5	C_6
$C_1 = (03,02)$	> 2.0					
$C_2 = (07,05)$	1.49	0.69				
$C_3 = (013,015)$	1.14	0.62	0.62			
$C_4 = (023,037)$	1.08	0.65	0.64	0.68		
$C_5 = (067,045)$	0.86	0.62	0.66	0.70	0.77	
$C_6 = (0147,0117)$	0.84	0.63	0.67	0.72	0.81	0.84

TABLE V
EXAMPLES OF SYMMETRIC PCC WITH EARLY CONVERGENCE. GAUSSIAN CHANNEL

PCC rate 1/2			
memory ν	(G_r, G)	BER at 0.5dB	pinch–off [dB]
4	(037,021)	—	0.53
4	(022,037)	2e-5	0.48
5	—	—	—
6	(0102,0147)	2e-5	0.48
6	(0110,0141)	1e-3	0.42 *)
*) 2nd intersection at $(I_A, I_E) \approx (0.93, 0.93)$ for 0.42dB			

(a)

PCC rate 1/3			
memory ν	(G_r, G)	BER at -0.2dB	pinch–off [dB]
4	(025,037)	3e-6	-0.22
5	(044,073)	2e-5	-0.22
6	(0111,0113)	1e-6	-0.24
6	(0120,0127)	2e-4	-0.25
6	(0120,0117)	3e-3	-0.34 +)
+) 2nd intersection at $(I_A, I_E) \approx (0.78, 0.78)$ for -0.34dB			

(b)

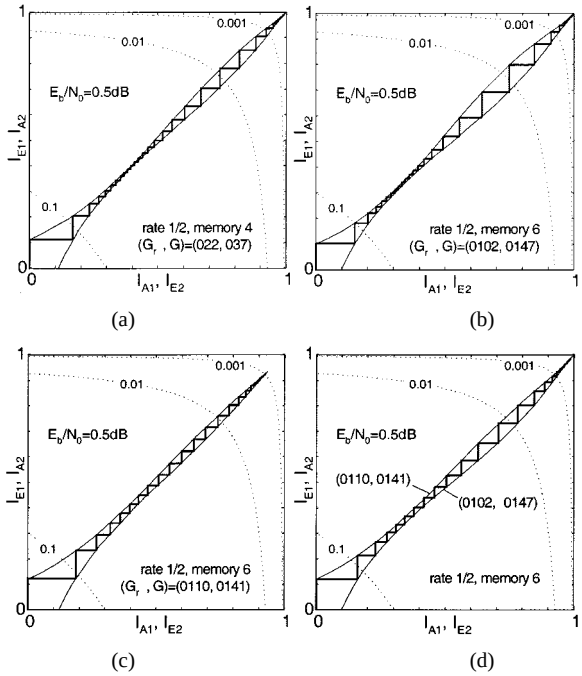

Fig. 12. Examples of decoding trajectories for three symmetric and one asymmetric rate $1/2$ PCC with turbo cliff below 0.5 dB (Gaussian channel); interleaver size 10^6 bits.

converging toward very low BER. This second threshold cannot be removed by using a larger interleaver; instead, a further increase of the E_b/N_0-value by about 0.4 dB is required. This observation for PCC is in analogy to the *stability condition* for LDPC codes, as described in [5]. The stability condition is a function of the code and channel parameters and has not yet been worked out for PCC.

As the code search results are based on the transfer characteristics of individual constituent codes we verified them by simulating the respective iterative decoders using an interleaving depth of 10^6 bits. Note that the BER given in Table V is averaged over just 10 blocks (i.e., 10^7 systematic bits, 40 iterations) and should merely be understood as an indication that convergence to low BER is possible.

From Fig. 12 we can see that the memory 6 code with polynomials (0110, 0141) has a fairly open bottleneck region at 0.5 dB, but the trajectory gets stuck at a BER of about 10^{-3}, owing to the intersection of both characteristics before reaching $(I_A, I_E) \approx (1, 1)$. We can cure this problem by combining it with the memory 6, (0102, 0147)-code to obtain both a fairly open bottleneck region and an open tunnel up to $(I_A, I_E) \approx (1, 1)$ (see bottom right EXIT chart of Fig. 12).

C. Verifying Pinch-Off Limits by BER Curves

To further confirm the threshold predictions of Section VI-A and the code search results of Section VI-B, we compare four different PCC of rate $1/2$ in the BER chart of Fig. 13. Using an interleaver size of 50 000 bits and simulating 10^7 information bits for each point of the BER curves contribute to achieving more reliable BER results than in the previous section. The relative order of the BER curves agrees well with the predicted E_b/N_0-threshold values; for larger interleaver size we find that

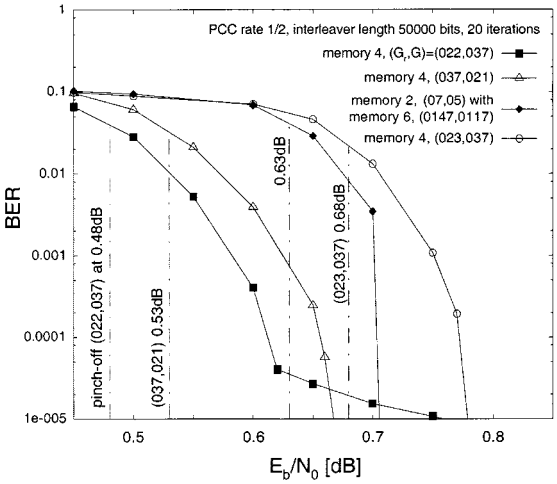

Fig. 13. BER curves and pinch-off limits for symmetric and asymmetric PCC of rate 1/2; interleaver size 50 000 bits, 20 iterations.

the turbo cliffs become more pronounced and approach the predicted pinch-off limits very closely; in addition to that, the BER floors are lowered. The rate 1/2 PCC with polynomials $(G_r, G) = (022, 037)$ is the best memory 4 code we found; it converges at lower E_b/N_0 than the classic memory 4 PCC with polynomials $(G_r, G) = (037, 021)$ [21]; however, the BER floor of the (022, 037)-code turns out to be higher. The BER curves of the symmetric PCC of Fig. 6 and the asymmetric PCC of Fig. 9 are given as additional references.

VII. Summary and Conclusion

Mutual information between transmitted systematic bits and extrinsic output of constituent decoders was found to be a useful measure for gaining insight into the convergence behavior of iterative decoding. The EXIT chart has been presented as an engineering tool for the design of iterative decoding schemes, in principle not limited to parallel concatenated codes. In the case of symmetric PCC the computation of transfer characteristics for only one constituent decoder turned out to be sufficient to predict the performance of the corresponding iterative decoder.

References

[1] S. Benedetto and G. Montorsi, "Unveiling turbo codes: Some results on parallel concatenated coding schemes," *IEEE Trans. Inform. Theory*, vol. 42, pp. 409–428, Mar. 1996.

[2] L. C. Perez, J. Seghers, and D. J. Costello, "A distance spectrum interpretation of turbo codes," *IEEE Trans. Inform. Theory*, vol. 42, pp. 1698–1709, Nov. 1996.

[3] T. Duman and R. Salehi, "New performance bounds for turbo codes," in *Proc. GLOBECOM*, Nov. 1997, pp. 634–638.

[4] T. J. Richardson and R. Urbanke, "The capacity of low-density parity-check codes under message-passing decoding," *IEEE Trans. Inform. Theory*, vol. 47, pp. 599–618, Feb. 2001.

[5] T. J. Richardson, A. Shokrollahi, and R. Urbanke, "Design of capacity-approaching irregular low-density parity-check codes," *IEEE Trans. Inform. Theory*, vol. 47, pp. 619–637, Feb. 2001.

[6] S. Y. Chung, G. D. Forney, T. J. Richardson, and R. Urbanke, "On the design of low-density parity-check codes within 0.0045 dB of the Shannon limit," *IEEE Commun. Lett.* , vol. 5, pp. 58–60, Feb. 2001.

[7] H. El Gamal and A. R. Hammons, "Analyzing the turbo decoder using the Gaussian approximation," *IEEE J. Select. Areas Commun.* , vol. 47, pp. 671–686, Feb. 2001.

[8] D. Divsalar, S. Dolinar, and F. Pollara, "Low complexity turbo-like codes," in *Proc. 2nd Int. Symp. Turbo Codes*, Sept. 2000, pp. 73–80.

[9] M. Peleg, I. Sason, S. Shamai, and A. Elia, "On interleaved, differentially encoded convolutional codes," *IEEE Trans. Inform. Theory*, vol. 45, pp. 2572–2582, Nov. 1999.
[10] S. ten Brink, "Convergence of iterative decoding," *Electron. Lett.*, vol. 35, no. 10, pp. 806–808, May 1999.
[11] ——, "Iterative decoding for multicode CDMA," in *Proc. IEEE VTC*, May 1999, pp. 1876–1880.
[12] ——, "Iterative decoding trajectories of parallel concatenated codes," in *Proc. 3rd IEEE/ITG Conf. Source Channel Coding*, Munich, Germany, Jan. 2000, pp. 75–80.
[13] L. Bahl, J. Cocke, F. Jelinek, and J. Raviv, "Optimal decoding of linear codes for minimizing symbol error rate," *IEEE Trans. Inform. Theory*, vol. 20, pp. 284–287, Mar. 1974.
[14] P. Robertson, E. Villebrun, and P. Hoeher, "A comparison of optimal and sub-optimal MAP decoding algorithms operating in the log domain," in *Proc. ICC*, June 1995, pp. 1009–1013.
[15] J. Hagenauer, E. Offer, and L. Papke, "Iterative decoding of binary block and convolutional codes," *IEEE Trans. Inform. Theory*, vol. 42, pp. 429–445, Mar. 1996.
[16] N. Wiberg, "Codes and decoding on general graphs," Ph.D. dissertation, Linköping Univ., Sweden, 1996.
[17] J. Hagenauer, P. Robertson, and L. Papke, "Iterative ('turbo') decoding of systematic convolutional codes with the MAP and SOVA algorithms," in *Proc. ITG Symp. on Source and Channel Coding*, Munich, Germany, 1994, pp. 21–29.
[18] T. M. Cover and J. A. Thomas, *Elements of Information Theory*. New York: Wiley, 1991.
[19] R. W. Hamming, *Coding and Information Theory*. Englewood Cliffs, NJ: Prentice-Hall, 1986.
[20] M. S. C. Ho, S. S. Pietrobon, and T. Giles, "Improving the constituent codes of turbo encoders," in *Proc. IEEE Globecom*, Sydney, Australia, Nov. 1998, pp. 3525–3529.
[21] C. Berrou, A. Glavieux, and P. Thitimajshima, "Near Shannon limit error-correcting coding and decoding: Turbo-codes," in *Proc. ICC*, May 1993, pp. 1064–1070.
[22] T. J. Richardson and R. Urbanke, "Thresholds for turbo codes," in *Proc. Int. Symp. Inform. Theory*, June 2000, p. 319.
[23] S. ten Brink, "Designing iterative decoding schemes with the extrinsic information transfer chart," *AEÜ Arch. Elektron. Übertragung.*, vol. 54, no. 6, pp. 389–398, Dec. 2000.
[24] I. S. Gradshteyn and I. M. Ryzhik, *Tables of Integrals, Series and Products*. New York: Academic, 1980.
[25] S. Benedetto, R. Garello, and G. Montorsi, "A search for good convolutional codes to be used in the construction of turbo codes," *IEEE Trans. Commun.*, vol. 46, pp. 1101–1105, Sept. 1998.

Stephan ten Brink received the Dipl.-Ing. degree in electrical engineering and information technology from the University of Stuttgart, Stuttgart, Germany, in 1997.

From 1997 to 2000 he was a research assistant with the Institute of Telecommunications, Stuttgart, working toward the doctoral degree. Since November 2000, he has been with the Wireless Research Lab of Bell Laboratories, Lucent Technologies, Holmdel, NJ. His research interests include multiuser detection, error correcting coding, and channel estimation for digital communication systems.